Bayesian Sonar Detection Performance Prediction With Source Position Uncertainty Using SWellEx-96 Vertical Array Data

Liewei Sha and Loren W. Nolte, *Life Senior Member, IEEE*

***Abstract*—Predicting sonar detection performance is important for the development of sonar systems. The classical sonar equation cannot accurately predict sonar detection performance because it does not incorporate the effect of ocean environmental and source position uncertainty. We propose an analytical receiver operating characteristic (ROC) expression that characterizes the performance of the optimal Bayesian detector in the presence of ocean environmental and source position uncertainty. The approach is based on a statistical model of the environment and a physical model of acoustic propagation, which translates ocean environmental and source position uncertainty to signal wavefront uncertainty. The analytical ROC expression developed in this paper is verified for source position uncertainty due to source motion using both simulated data and real data collected during the Shallow Water Evaluation Cell Experiment (SWellEx-96). The results showed that the primary effect of source position uncertainty on optimal sonar detection performance is captured by the rank that corresponds to the significant eigenvalues of the signal matrix, an ensemble of replica signal wavefronts (normalized acoustic pressure vector) at the receiving array. The results also showed that the proposed ROC expression provides a realistic detection performance prediction for the Bayesian detector for source position uncertainty using real data. The proposed approach to sonar detection performance prediction is much simpler and faster than those using conventional Monte Carlo approaches.**

***Index Terms*—Bayesian detection, performance prediction, source position uncertainty.**

I. Introduction

THE passive detection and localization of submerged targets in an ocean environment can be challenging because of the complicated environment. For example, there is uncertainty in the movement of an acoustic source. In addition, the ocean parameters that affect acoustic propagation, such as water depth and sound-speed profile, have uncertainty both spatially and temporally. The set of source position parameters together with the propagation channel parameters constitute an uncertain environment. As a result of this environmental uncertainty, there is signal wavefront uncertainty at the receiving array which can cause great performance degradation in sonar detection and localization algorithms that rely on accurate prediction of the signal wavefront [1]–[3]. It is of great interest to characterize and predict optimal sonar detection and localization performance in the presence of environmental source position uncertainty and the resultant wavefront uncertainty.

Among the detection and localization algorithms that are robust to environmental uncertainty, the physics-based Bayesian approach has been proposed [4]–[7]. This approach merges statistical modeling of environmental uncertainty with physical modeling of the propagation medium to achieve optimal sonar performance in the presence of environmental uncertainty. Previous works include the optimal uncertain field processor (OUFP) [4] for source localization, full-field optimum detection in a random wave scattering environment [6], the optimal wideband active detector [7], and the Bayesian detectors [5], [8], [9]. The physics-based Bayesian approach enables a full incorporation of uncertainty at the environmental parameter level, where the stochastic descriptions can be obtained much easier and more directly than at the signal wavefront level.

The performance characterization of the Bayesian detection algorithms is difficult. Typically, Monte Carlo evaluation techniques have been used to obtain the receiver operating characteristic (ROC) for the physics-based Bayesian detection algorithms [5]–[7], which can be computationally intensive. In [8], approximate analytical ROC expressions were developed, which incorporate the effect of ocean environmental uncertainty and source position uncertainty. The analytical ROC expressions were verified using 21 scenarios extended from an U.S. Naval Research Laboratory (NRL) benchmark shallow-water model, e.g., uncertain water depth scenario, uncertain sound-speed profile scenario, uncertain source depth scenario, scenario of general uncertainty in propagation channel parameters, etc. Various ranges of uncertainties were considered [8]. In [9], the effect of interference in uncertain environments was incorporated in the analytical detection performance prediction, which was checked using simulated data generated from an NRL benchmark shallow-water model. In [8] and [9], the transmitted signal was assumed to have a random amplitude following a complex Gaussian distribution, while in this paper the transmitted signal is assumed to have a fixed real amplitude and a random phase. As compared to [8], the approximate ROC expression developed in this paper is more accurate if the source level is fixed during the observation interval, as assumed with the Shallow Water Evaluation Cell Experiment (SWellEx-96) data. However, the main contribution of this paper is to verify the approximate ROC expression using the SWellEx-96 data. In

Manuscript received February 26, 2004; revised December 23, 2005; accepted January 8, 2006. This work was supported by the ONR Uncertainty DRI Contract 313-4007-22302. **Guest Editor: W. S. Hodgkiss.**

L. Sha was with Electrical and Computer Engineering Department, Duke University, Durham, NC 27708-0291 USA. She is now with Magnetic Resonance Imaging, GE Healthcare Technology, Waukesha, WI 53188 USA (e-mail: liewei.sha@med.ge.com).

L. W. Nolte is with Electrical and Computer Engineering Department, Duke University, Durham, NC 27708-0291 USA (e-mail: lwn@ee.duke.edu).

Digital Object Identifier 10.1109/JOE.2006.875263

this data set, there is little ocean environmental uncertainty, but mainly source position uncertainty due to source motion. The results show that detection performance depends on the amount of source position uncertainty, as captured by the number of the dominant eigenvalues of the signal matrix, as well as the signal-to-noise ratio (SNR) at the receivers. Using these two fundamental parameters, the rank of the signal matrix and the array-level SNR, an analytical expression for the ROC is obtained that provides a very fast performance prediction for the Bayesian detector. It is a more realistic performance prediction than obtained using the classic sonar equation, which does not take into account environmental or source position uncertainty.

The paper is organized as follows. The detection problem and the signal model are formulated in Section II. The Bayesian algorithm for the detection of the signal with random phase in the presence of environmental uncertainty is presented in Section III. The approximate ROC expression for the Bayesian detector is developed in Section IV. In Section V, the alternative detectors are defined. In Section VI, simulated data generated from the SWellEx-96 environmental model as well as SWellEx-96 experimental data are used to illustrate the analytical ROC expression for the Bayesian detector, and to analyze the effect of source position uncertainty on optimal sonar detection performance.

II. Formulation of the Detection Problem

The detection problem is formulated using a statistical model of environmental uncertainty and a physics-based signal model.

In the environmental uncertainty model, the propagation channel parameters $\mathbf{\Psi}$ and the source position parameters $\mathbf{S}$ are quantified by assigning statistically independent uniform probability density functions (pdf) $p(\mathbf{\Psi})$ and $p(\mathbf{S})$. Although the uniform pdf is used, a different pdf could be assigned if it better represented the *a priori* knowledge.

It is assumed that the received signal is a spatial vector in the frequency domain, narrowband, centered at a known frequency f_0. The received signal consists of the signal wavefront, i.e., the normalized acoustic pressure vector, and a complex amplitude. The signal wavefront $\mathbf{s}(\mathbf{\Psi},\mathbf{S})$ is given by

$$\mathbf{s}(\mathbf{\Psi},\mathbf{S}) = \frac{\mathbf{H}(\mathbf{\Psi},\mathbf{S})}{||\mathbf{H}(\mathbf{\Psi},\mathbf{S})||} \tag{1}$$

where $\mathbf{H}(\mathbf{\Psi},\mathbf{S})$ is the frequency-domain ocean acoustic transfer function, or replica field, sampled at an arbitrary receiving array of N sensors, given ocean parameters $\mathbf{\Psi}$ and source position parameters $\mathbf{S}$. Here $\|\cdot\|$ means the two-norm on a complex vector space.

The replica field generated by a point source at depth z_s and range r_s is computed using normal mode theory [10]

$$p(z_i;r_s,z_s) = p_0 \sum_{m=1}^{K} \mathbf{\Phi}_m(z_s,r_s)\mathbf{\Phi}_m(z_i)\frac{e^{-jk_m r_s}}{\sqrt{k_m r_s}} \tag{2}$$

where (z_s,r_s) is the source position at depth z_s and range r_s, referred to as $\mathbf{S}$ for simplicity, z_i is the depth of the ith receiver, and p_0 is a normalization constant. The number of propagating acoustic modes is represented by K. The terms k_m and $\mathbf{\Phi}_m$ are the mth eigenvalue and eigenfunction of the Sturm–Louisville problem, which can be calculated using Porter's KRAKEN code [11].

The complex amplitude is denoted by $\mu e^{j\theta}$, where θ is a random variable uniformly distributed from 0 to 2π, used to model the unknown phase of the signal emitted by an acoustic source. The scalar μ is the product of the norm of the acoustic transfer function $\|\mathbf{H}(\mathbf{\Psi},\mathbf{S})\|$ and the amplitude of the signal emitted by the acoustic source a. The source amplitude and the norm of the acoustic transfer function are merged together because the effects of these two components on the detection performance are indistinguishable. Here it is assumed that μ is a known variable rather than a Rayleigh random variable assumed in [8]. The known variable model is appropriate if the source level does not change during the observation interval and a good estimate of the amplitude of the received signal is available.

The signal wavefront is a function of the continuous random variables $\mathbf{\Psi}$ and $\mathbf{S}$. To quantitatively predict the performance of the detection algorithms in an uncertain environment, a discrete representation of the uncertain signal wavefront is needed. A matrix composed of M realizations of the signal wavefront due to environmental uncertainties is considered, which is defined by applying Monte Carlo sampling techniques. This matrix is referred to as the signal matrix $\mathfrak{R}$ [8]

$$\begin{aligned}\mathfrak{R} &= [\mathbf{s}_1,\mathbf{s}_2,\ldots\mathbf{s}_M] \\ &= [\mathbf{s}((\mathbf{\Psi},\mathbf{S})_1),\mathbf{s}((\mathbf{\Psi},\mathbf{S})_2),\ldots\mathbf{s}((\mathbf{\Psi},\mathbf{S})_M)]\end{aligned} \tag{3}$$

where $(\mathbf{\Psi},\mathbf{S})_{i,i=1\ldots M}$ corresponds to the ith realization of the environmental parameters $(\mathbf{\Psi},\mathbf{S})$, which results from the uniform pdf $p(\mathbf{\Psi})p(\mathbf{S})$ assumed for the *a priori* uncertainty range $\Omega_{\mathbf{\Psi}}$ and $\Omega_{\mathbf{S}}$. If M is large enough, the signal matrix is a good representation of realizations of uncertain signal wavefronts. The criterion for determining M is problem dependent. Usually, M should be greater than the number of propagating modes K so that independent information carried by the propagation modes can be captured by the samples of the signal wavefronts. In this paper, $M = 120$ is used. This value has been checked using many simulation examples to show that further increase in M does not significantly change the ROC performance predictions discussed in this paper.

The detection problem is formulated as a binary hypotheses testing problem. For an arbitrary array of N sensors, the observation $\mathbf{r}$ is an $N\times 1$ spatial vector in the frequency domain, obtained using a one dimensional narrowband Fourier transform of the snapshot for each of the N array elements. A snapshot consists of O consecutive time samples. Given the observation, we must decide between two hypotheses: The "null" hypothesis H_0 and the "signal present" hypothesis H_1, in the presence of environmental uncertainty

$$\begin{aligned} H_1 &: \mathbf{r} = \mu e^{j\theta}\mathbf{s}(\mathbf{\Psi},\mathbf{S}) + \mathbf{n}_0 \\ H_0 &: \mathbf{r} = \mathbf{n}_0 \\ \mathbf{n}_0 &\sim \mathcal{N}(0, 2\sigma_n^2\mathbf{I}_N) \\ \mathbf{\Psi} &\sim p(\mathbf{\Psi}), \mathbf{S} \sim p(\mathbf{S}) \end{aligned} \tag{4}$$

where the noise field $\mathbf{n}_0$ is modeled by a $N\times 1$ spatial complex Gaussian vector in the frequency domain with zero mean and

covariance matrix $2\sigma_n^2\mathbf{I}_N$. The symbol $\mathbf{I}_N$ means the identity matrix with size N and the symbol $\sim$ means "distributed as."

Equation (4) is the formulation of the detection problem in a continuous form. By applying the concept of the signal matrix as in (3), the detection problem can also be formulated in a discrete form

$$\begin{aligned} H_1 &: \mathbf{r} = \mu e^{j\theta}\mathbf{s}_i + \mathbf{n}_0, \qquad i \in 1 \dots M \\ H_0 &: \mathbf{r} = \mathbf{n}_0, \qquad \mathbf{n}_0 \sim \mathcal{N}(0, 2\sigma_n^2\mathbf{I}_N) \end{aligned} \tag{5}$$

where $\mathbf{s}_i$ is an arbitrary column of the signal matrix. The probability of selecting $\mathbf{s}_i$ among M columns of the signal matrix is $1/M$.

III. Bayesian Detector

Here we consider wavefront uncertainty caused by uncertain environmental parameters. We derive the Bayesian detector that incorporates the *a priori* information of the environmental parameters, and develop an approximate analytical ROC expression for the performance of the optimal Bayesian detector.

The derivation of the Bayesian detector begins with the likelihood ratio, which requires integration over the uncertain environmental parameters for the H_1 hypothesis, and is given by

$$\begin{aligned} \lambda(\mathbf{r}) &= \frac{\int_{\mathbf{\Psi}}\int_{\mathbf{S}} d\mathbf{\Psi} d\mathbf{S} p(\mathbf{r} \mid H_1, \mathbf{\Psi}, \mathbf{S}) p(\mathbf{\Psi}) p(\mathbf{S})}{p(\mathbf{r} \mid H_0)} \\ &= \int_{\mathbf{\Psi}}\int_{\mathbf{S}} d\mathbf{\Psi} d\mathbf{S} \lambda(\mathbf{r} \mid \mathbf{\Psi}, \mathbf{S}) p(\mathbf{\Psi}) p(\mathbf{S}) \end{aligned} \tag{6}$$

where $\lambda(\mathbf{r} \mid \mathbf{\Psi}, \mathbf{S})$ is the conditional likelihood ratio. The latter can be derived from the pdf of the data conditional to the H_0 hypothesis and the H_1 hypothesis given known environmental parameters $\mathbf{\Psi}$ and $\mathbf{S}$

$$p(\mathbf{r} \mid H_0) = \frac{1}{(2\pi\sigma_n^2)^N} e^{-(\mathbf{r}^\dagger \mathbf{r}/2\sigma_n^2)} \tag{7}$$

$$\begin{aligned} p(\mathbf{r} \mid H_1, \mathbf{\Psi}, \mathbf{S}) &= \frac{1}{2\pi}\int_0^{2\pi} d\theta p(\mathbf{r} \mid \theta, H_1, \mathbf{\Psi}, \mathbf{S}) \\ &= \frac{1}{2\pi}\int_0^{2\pi} d\theta \frac{1}{(2\pi\sigma_n^2)^N} \\ &\quad \times e^{-(r-\mu e^{j\theta}\mathbf{s}(\mathbf{\Psi},\mathbf{S}))^\dagger (r-\mu e^{j\theta}\mathbf{s}(\mathbf{\Psi},\mathbf{S}))/2\sigma_n^2} \\ &= \frac{1}{(2\pi\sigma_n^2)^N} e^{-(\mathbf{r}^\dagger\mathbf{r}/2\sigma_n^2) - (\mathrm{SNR}(\mathbf{\Psi},\mathbf{S})/2)} \\ &\quad \times I_0\left(\frac{\mu}{\sigma_n^2}|\mathbf{r}^\dagger \mathbf{s}(\mathbf{\Psi}, \mathbf{S})|\right) \end{aligned} \tag{8}$$

where $I_0(\cdot)$ is the modified zero-order Bessel function of the first kind. The SNR at the receivers $\mathrm{SNR}(\mathbf{\Psi}, \mathbf{S})$ is defined as

$$\mathrm{SNR}(\mathbf{\Psi}, \mathbf{S}) = |a|^2 \frac{||\mathbf{H}(\mathbf{\Psi}, \mathbf{S})||^2}{\sigma_n^2}. \tag{9}$$

The SNR includes the factors of the square of the source amplitude, the diffuse noise variance, and the array gain. It is not the element-level SNR but an array-level SNR, where the signal power component is the sum of the signal powers from each element of the array.

Combining (7) and (8) yields the conditional likelihood ratio

$$\lambda(\mathbf{r} \mid \mathbf{\Psi}, \mathbf{S}) = e^{-\mathrm{SNR}(\mathbf{\Psi},\mathbf{S})/2} I_0\left(\frac{\mu}{\sigma_n^2}|\mathbf{r}^\dagger \mathbf{s}(\mathbf{\Psi}, \mathbf{S})|\right). \tag{10}$$

The conditional likelihood ratio, which is a kernel in the likelihood ratio for signal wavefront uncertainty, is consistent with the optimal Bayesian test for detection of signal with unknown phase but known signal wavefront in the literature ([12, eq. 33.11] and [13, eq. 13]).

Finally, the Bayesian detector for the detection of a signal with unknown phase in an uncertain environment in diffuse noise is given by (6), (10), and (9).

To facilitate the computation of the likelihood ratio and the derivation of the ROC expression, a discrete likelihood ratio is obtained by applying the concept of the signal matrix

$$\begin{aligned} \lambda(\mathbf{r}) &= \frac{1}{M}\sum_{i=1}^{M} \lambda_i \\ \lambda_i &= e^{-\mathrm{SNR}_i/2} I_0\left(\frac{\mu}{\sigma_n^2}|\mathbf{r}^\dagger \mathbf{s}_i|\right) \\ \mathrm{SNR}_i &= \mathrm{SNR}((\mathbf{\Psi}, \mathbf{S})_i). \end{aligned} \tag{11}$$

IV. Performance of the Bayesian Detector

The detection problem defined in (5) can be placed into a more general framework, the detection of M-correlated signals in Gaussian noise. An accurate analytical ROC expression for the Bayesian detector for the M-correlated signal detection problem is formidable. Here, we develop an approximate analytical ROC expression for the M-correlated signal detection problem, where the correlated signals consist of realizations of the signal wavefront due to uncertain environmental parameters. A similar general derivation technique was used in [8] for the case where the source amplitude was also unknown, so we limit our presentation here to the major steps.

The derivation of the ROC involves the following steps.

1) Approximate the optimal decision rule to be "if $\lambda_i \geq \beta$ for any $i \in 1 \dots M$, decide H_1 and if $\lambda_i < \beta$ for all $i = 1 \dots M$, decide H_0." With this approximation, the probability of false alarm (P_F) and the probability of detection (P_D) can be expressed as integrations of the available joint probability density function of λ_i rather than the unknown probability density function of λ

$$\begin{aligned} P_F(\beta) &= 1 - P(\lambda_i < \beta, i = 1 \dots M \mid H_0) \\ P_D(\beta) &= 1 - P(\lambda_i < \beta, i = 1 \dots M \mid H_1) \end{aligned} \tag{12}$$

where β is the decision threshold. This approximation was suggested in a different context in [12].

2) Assume the array-level SNR is constant over environmental uncertainty. With this assumption, λ_i can be replaced by its monotonic function $|\mathbf{r}^\dagger \mathbf{s}_i|$ in the decision rule

$$\begin{aligned} P_F(\beta') &= 1 - P(|\mathbf{r}^\dagger \mathbf{s}_i|^2 < \beta', i = 1 \dots M \mid H_0) \\ P_D(\beta') &= 1 - P(|\mathbf{r}^\dagger \mathbf{s}_i|^2 < \beta', i = 1 \dots M \mid H_1) \end{aligned} \tag{13}$$

where β' is the new decision threshold, given by $\beta' = I_0^{-1}(\beta e^{\mathrm{SNR}/2})\sigma_n^2/\mu$, and $I_0^{-1}(\cdot)$ is the inverse function of $I_0(\cdot)$.

3) Estimate the rank of the signal matrix R as the number of significant eigenvalues of the signal matrix. Since

the covariance matrix of the data $\mathbf{r}$ for the H_1 hypothesis is singular, which makes the formulation of the pdf difficult, it is necessary to reduce the dimensionality of the signal and noise vectors from N to R, so that the covariance matrix of the new data is nonsingular. Similar to the steps in [8] and [14], multiplying the unitary matrix $\mathbf{U}$ to both sides of (5) yields a transformed binary detection model, where $\mathbf{U}$ is $N \times N$ size, generated from a singular value decomposition of the signal matrix. Denote the significant R columns of $\mathbf{U}$ by $\mathbf{U}_1$, which is associated with the R significant eigenvalues, and denote the remaining columns by $\mathbf{U}_2$. Since the products of $\mathbf{U}_2$ with the signal (or noise) vectors contain little information (whether the signal is present or not), these products can be ignored without affecting the detection performance. The products of $\mathbf{U}_1$ with the data, signal, and noise vectors are the new vectors in reduced dimensionality: $\mathbf{u} = \mathbf{U}_1^{\dagger}\mathbf{r}$, $\mathbf{v}_i = \mathbf{U}_1^{\dagger}\mathbf{s}_i$, $i = 1 \ldots M$, and $\mathbf{w} = \mathbf{U}_1^{\dagger}\mathbf{n}$.

Both P_D and P_F can be expressed as a R-dimensional integral of the pdf of the data $\mathbf{u}$ conditional to the H_1 or H_0 hypotheses

$$\begin{aligned} P_F(\beta') &= 1 - P(|\mathbf{u}^{\dagger}\mathbf{v}_i|^2 < \beta', i = 1 \ldots M \mid H_0) \\ &= 1 - \int_{|\mathbf{u}^{\dagger}\mathbf{v}_i|^2 < \beta', i = 1 \ldots M} d\mathbf{u} p(\mathbf{u} \mid H_0) \\ P_D(\beta') &= 1 - P(|\mathbf{u}^{\dagger}\mathbf{v}_i|^2 < \beta', i = 1 \ldots M \mid H_1) \\ &= 1 - \int_{|\mathbf{u}^{\dagger}\mathbf{v}_i|^2 < \beta', i = 1 \ldots M} d\mathbf{u} p(\mathbf{u} \mid H_1). \end{aligned} \tag{14}$$

4) Approximate the integration domain for the computation of the probability of detection.

Replacing $\mathbf{r}$ and N with $\mathbf{u}$ and R, respectively, in (7) yields the pdf of the data $\mathbf{u}$ conditional to the H_0 hypothesis

$$p(\mathbf{u} \mid H_0) = \frac{1}{(2\pi\sigma_n^2)^R} e^{-(\mathbf{u}^{\dagger}\mathbf{u}/2\sigma_n^2)}. \tag{15}$$

Replacing $\mathbf{s}(\mathbf{\Psi}, \mathbf{S})$ and N with $\mathbf{v}_m$ and R in (8), and integrating over M signal realizations yields the pdf of the data $\mathbf{u}$ conditional to the H_1 hypothesis and $\mathbf{v}_m$, the signal vector transformed from the mth column of the signal matrix

$$\begin{aligned} p(\mathbf{u} \mid H_1) &= \frac{\sum_{m=1}^{M} p(\mathbf{u} \mid H_1, \mathbf{v}_m)}{M} \\ p(\mathbf{u} \mid H_1, \mathbf{v}_m) &= \frac{1}{(2\pi\sigma_n^2)^R} e^{-(\mathbf{u}^{\dagger}\mathbf{r}/2\sigma_n^2) - (\mathrm{SNR}/2)} \\ &\quad \times I_0\left(\frac{\mu}{\sigma_n^2}|\mathbf{u}^{\dagger}\mathbf{v}_m|\right). \end{aligned} \tag{16}$$

Substituting (16) in (14) generates the P_D

$$\begin{aligned} P_D(\beta') &= \sum_{m=1}^{M} \frac{P_{Dm}}{M} \\ P_{Dm}(\beta') &= -\int_{|\mathbf{u}^{\dagger}\mathbf{v}_i|^2 < \beta', i = 1 \ldots M} d\mathbf{u} p(\mathbf{u} \mid H_1, \mathbf{v}_m) \end{aligned} \tag{17}$$

where P_{Dm} is probability of detection using $\mathbf{v}_m$ as the reference signal. Assume $\mathbf{v}_1$ as the reference signal for the derivation of P_{D1}. Let $\mathbf{P} = [\mathbf{v}_1\ \mathbf{T}]$ be an $R \times R$ matrix whose columns form a complete orthonormal basis, where $\mathbf{T}$ is of size $(R-1) \times R$, generated by the Gram–Schmidt orthogonalization procedure.

Given $\mathbf{v}_1$, the data vector $\mathbf{u}$ can be transformed to vector $\mathbf{z}$ through $\mathbf{P}$ to facilitate the derivations of P_F and P_D. Since $\mathbf{P}$ is orthonormal, substituting $\mathbf{z} = \mathbf{r}\mathbf{P}$ in (15) and (16) yields

$$\begin{aligned} p(\mathbf{z} \mid H_0) &= \frac{1}{(2\pi\sigma_n^2)^R} e^{-(\mathbf{z}^{\dagger}\mathbf{z}/2\sigma_n^2)} \\ p(\mathbf{z} \mid H_1, \mathbf{v}_1) &= \frac{1}{(2\pi\sigma_n^2)^R} e^{-(\mathbf{z}^{\dagger}\mathbf{z}/2\sigma_n^2) - (\mathrm{SNR}/2)} \\ &\quad \times I_0\left(\frac{\mu}{\sigma_n^2}|\mathbf{z}_1|\right) \end{aligned} \tag{18}$$

where $\mathbf{z}_1$ is the first component of $\mathbf{z}$ and $\mathbf{z}_{i, i=2 \ldots R}$ are the rest components of $\mathbf{z}$.

Substituting (18) and $\mathbf{u} = \mathbf{z}\mathbf{P}^{-1}$ in (14) yields

$$\begin{aligned} P_F(\beta') &= 1 - \int_D d\mathbf{z} \frac{1}{(2\pi\sigma_n^2)^R} e^{-(\mathbf{z}^{\dagger}\mathbf{z}/2\sigma_n^2)} \\ P_{D1}(\beta') &= 1 - \int_D d\mathbf{z} \frac{1}{(2\pi\sigma_n^2)^R} e^{-(\mathbf{z}^{\dagger}\mathbf{z}/2\sigma_n^2)(\mathrm{SNR}/2)} \\ &\quad \times I_0\left(\frac{\mu}{\sigma_n^2}|\mathbf{z}_1|\right) \end{aligned} \tag{19}$$

where the domain of the integration is $D = \{|\mathbf{z}^{\dagger}\mathbf{P}^{-\dagger}\mathbf{v}_i|^2 < \beta', i = 1 \ldots M\}$, which is an irregular convex body in R space. Although an accurate P_F and P_D can be obtained with intensive Monte Carlo computations, it is difficult to derive closed-form expressions for P_F and P_D, because of the irregularity of the integration domain. Similar to [8], we define a regular convex-body $C = \{|\mathbf{z}_i|^2 < \gamma, i = 1 \ldots R\}$ to replace the irregular integral domain $D = \{|\mathbf{z}^{\dagger}\mathbf{P}^{-H}\mathbf{s}_i|^2 < \beta', i = 1 \ldots M\}$. Considering the integration functions are Gaussian for both P_F and P_D, whose energy is concentrated on the origin, the approximation error due to moderate integration domain differences that are close to the boundary can be moderate. The accuracy of this approximation, in terms of the final goal of obtaining the ROC, is verified in the simulation section. Regardless of the approximation in the integration domain, the P_F and P_D approximation errors are zero at $\mathrm{SNR} = 0$ and $\mathrm{SNR} = \infty$.

Integrating the right side of (19) using domain C for both P_F and P_D generates

$$\begin{aligned} P_F(\gamma) &\approx 1 - \left(1 - \exp\left(\frac{-\gamma}{2\sigma_n^2}\right)\right)^R \\ P_{D1}(\gamma) &\approx 1 - \left(1 - Q\left(\sqrt{\mathrm{SNR}}, \sqrt{\frac{\gamma}{\sigma_n}}\right)\right) \\ &\quad \times \left(1 - \exp\left(\frac{-\gamma}{2\sigma_n^2}\right)\right)^{R-1} \end{aligned} \tag{20}$$

where $Q(,)$ is the Q function defined by Marcum and Swerling [15]

$$Q(\alpha, \beta) = \int_{\beta}^{\infty} v e^{-(v^2 + \alpha^2/2)} I_0(\alpha v) dv. \tag{21}$$

Since the approximate P_{D1} expression is independent of the reference signal $\mathbf{v}_1$, the approximate P_D expression is the same

as the P_{D1} expression. Finally, combining P_F and P_D in (20) yields

$$P_D \approx 1 - \left(1 - Q\left(\sqrt{\mathrm{SNR}}, -\sqrt{2\log(1-(1-P_F)^{1/R})}\right)\right) \times (1-P_F)^{(R-1)/R} \quad (22)$$

where R is the rank of the signal matrix and the SNR is assumed constant in the derivation. In real applications, we estimate the rank of the signal matrix by counting the number of the eigenvalues of the signal matrix which exceed a threshold. Using a threshold of 5% of the maximum eigenvalue gives consistent agreement between Monte Carlo simulation results and the analytical expression for the ROC. Empirical results suggest that the optimal detection performance is not highly sensitive to the exact setting of this threshold. The SNR can be replaced by the average SNR over the realizations of the uncertain environment

$$\mathrm{SNR} = \frac{1}{M}\sum_{i=1}^{M} \mathrm{SNR}((\mathbf{\Psi}, \mathbf{S})_i). \quad (23)$$

The averaged SNR approximation and the resultant optimal Bayesian predictor might fail for a short vertical array or horizontal array, because the received signal energy is sensitive to source range variation.

Both the optimal Bayesian predictor and the Monte Carlo performance evaluation approach require the *a priori* knowledge on the signal matrix, i.e., the set of replica vectors due to uncertain environmental parameters. It is computationally intensive to obtain the replica vectors. Considering the mean-ocean environmental parameters change slowly, it is possible to precalculate the replica vectors for interested source regions and worst-case environmental uncertainty. Assume the signal matrix is precalculated, the computational speed improvement of the analytical approach over the Monte Carlo approach is significant. The primary computational cost for the Monte Carlo approach is the generation of the samples of the likelihood ratio for each hypothesis, which is about $O(LMN)$, where L is the number of samples, M is the number of columns in the signal matrix, and N is the number of array sensors. The primary computational cost for the optimal Bayesian predictor is the computation of the eigenvalues, to estimate the approximate rank of the signal matrix, which is $O(N^3)$ [16], [17]. Typically, M is greater than N, and L is above 1000 to achieve a precision in P_D and P_F of about 0.001, which in turn is about ten times greater than N. Therefore, the analytical approach speedup is typically more than an order of magnitude over the Monte Carlo approach given the precalculated signal matrix.

V. Alternative Detectors

Three alternative detection algorithms are presented: The matched-ocean detector, the mean-ocean detector, and an energy detector. The matched-ocean detector and the mean-ocean detector use the same form of the test statistic, a modified version of the conventional Bartlett processor [10], [18]. The difference between these two detectors is the level of the *a priori* knowledge of the environmental uncertainty they utilize. The matched-ocean detector uses the signal wavefront that completely matches with the data. Its performance prediction provides an upper bound for a nonrealistic ideal situation. The mean-ocean detector uses the signal wavefront computed from the mean values of the environmental parameters.

For the matched-ocean detector, the environmental parameters $\mathbf{\Psi}$ and $\mathbf{S}$ are assumed known *a priori*. The matched-ocean detector is implemented by a monotonic function of the likelihood ratio, which is also optimal

$$\lambda' = |\mathbf{r}^\dagger \mathbf{s}(\mathbf{\Psi}, \mathbf{S})|. \quad (24)$$

The performance of the matched-ocean detector can be obtained by substituting $R = 1$ in (22), since the signal matrix only has one column, the known signal wavefront $\mathbf{s}(\mathbf{\Psi}, \mathbf{S})$

$$P_D = Q(\sqrt{\mathrm{SNR}}, -\sqrt{2\log(P_F)}). \quad (25)$$

The mathematical expressions for the matched-ocean detector as in (24) and its performance shown in (25) are similar to the expressions for the optimal Bayesian detector for the detection of a signal with unknown phase but known wavefront in Gaussian noise [12], [13].

The mean-ocean detector assumes a deterministic ocean equal to the mean ocean environment. The test statistic is given by

$$\lambda' = |\mathbf{r}^\dagger \mathbf{s}_{\mathrm{mean}}| \quad (26)$$

where $\mathbf{s}_{\mathrm{mean}}$ indicates the signal wavefront computed from the mean values of the environmental parameters.

The energy detector represents the algorithms that do not utilize the *a priori* knowledge of the environment at all. The test statistic of the energy detector is

$$\lambda' = |\mathbf{r}^\dagger \mathbf{r}|. \quad (27)$$

VI. Results: SWellEx-96 Simulations and Experimental Data

The data collected from event S5 of the SWellEx-96 experiment was used to demonstrate the proposed approximate analytical ROC expression. The SWellEx-96 experiment was conducted in May 1996, west of Point Loma in San Diego, CA [19]. This site is a shallow-water channel approximately 200 m in depth with a relatively flat bottom and a downward refracting sound-speed profile. Fig. 1 shows the environmental model to generate the replica field. This model also consists of a source at about 15-m deep, traveling in the nearby area, and a 21-element vertical line array (VLA) spaced over a 118-m aperture above the ocean floor. Fig. 5 is a map of the source track during event S5 with square marks every 5 min.

The uncertainties in the channel parameters are insignificant, because this site has been extensively studied and a detailed geoacoustic database and model exists. In addition, water-column sound-speed data is provided through a conductivity, temperature, depth (CTD) survey during the SWellEx-96 experiment. However, the acoustic source was moving, which caused variations of the signal wavefronts at the receiving array. In an ideal matched scenario, the precise source position is available so that the varying signal wavefront can be accurately predicted. Consequently, the Bayesian detector can be considered as the matched-ocean detector that provides a performance upper bound. However, in a realistic circumstance,

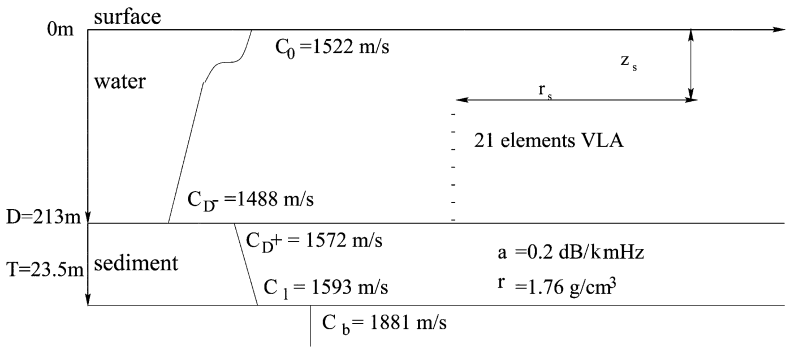

Fig. 1. Shallow-water environmental configuration for the SWellEx-96 experiment.

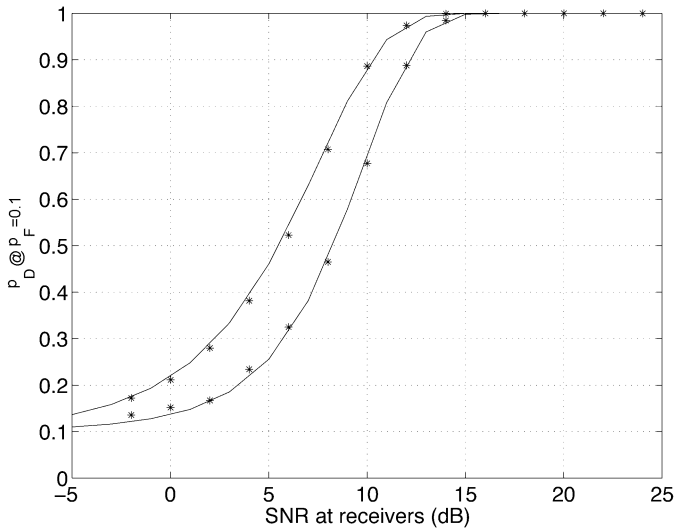

Fig. 2. Comparison of the analytical and experimental performance predictions for the Bayesian detector with simulated data, by plotting P_D as a function of the SNR at the receivers, for $P_F = 0.1$. Solid: analytical approach. Star: Monte Carlo approach. Left: Scenario A. Right: Scenario C (Table I).

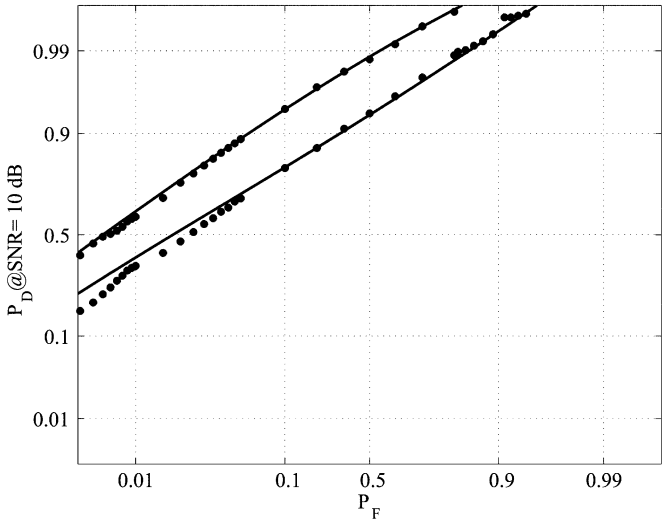

Fig. 3. Comparison of analytical and experimental performance predictions for the Bayesian detector with simulated data, by plotting P_D as a function of P_F, for about 10-dB SNR at the receivers. Solid: analytical approach. Star: Monte Carlo approach. Upper: Scenario A. Lower: Scenario C (Table I).

the source position is usually uncertain, which causes detection performance degradation. Since we know the source track during the SWellEx-96 experiment from the global positioning system (GPS) data, both ideal and realistic scenarios can be implemented for the verification of the analytical ROC expression and the analysis of the effect of source position uncertainty on detection performance.

Before presenting results using the experimental data, the accuracy of the approximate analytical ROC expression is verified using simulated data with the same SWellEx-96 environmental and acoustic propagation models. It is instructive to provide both the simulation results and the experimental results. The simulated results check the approximations used for deriving the analytical ROC expression. The experimental data results test the signal and noise models.

A. Simulation Results

Using the simulated data, the approximate analytical ROC expression is verified by comparing its prediction results with those obtained using Monte Carlo evaluations. The resultant P_D is plotted as a function of SNR, P_F, and source range uncertainty in Figs. 2–4.

Four scenarios (A–D) are listed in Table I, defined by the *a priori* region (range, depth) over which a source is located. The source position is assumed fixed during the observation and detection interval of one "snapshot." Whether the source is stationary or moving across snapshots does not affect the performance of the proposed detection algorithm.

The simulated data was generated using Monte Carlo sampling techniques over realizations of the source position, diffuse noise, and the phase of the transmitted signal, based on the data model as in (4), where the source frequency is assumed to be 109 Hz. The channel parameters are denoted in Fig. 1. Both the analytical approach and the Monte Carlo approach assume that the region of the source position, the received signal amplitude μ, and diffuse noise variance σ_n^2 were known *a priori*. Both approaches use the same signal matrix that consist of realizations of the signal wavefronts (normalized replica fields) due to the source positions uniformly distributed in the *a priori* region. A 750-m (range) $\times$ 4-m (depth) region is equally divided into grid units with about 19 m in range and 2 m in depth to generate total of 120 source positions. In using the Monte Carlo

TABLE I
SCENARIOS OF SOURCE POSITION UNCERTAINTY FOR SIMULATED DATA

scenarios	source range	range of source range uncertainty	source depth
A	3300 m	0 m	15±2 m
B	from 3300 m to 3044 m	256 m	15±2 m
C	from 3300 m to 2750 m	550 m	15±2 m
D	from 3300 m to 2276 m	1034 m	15±2 m

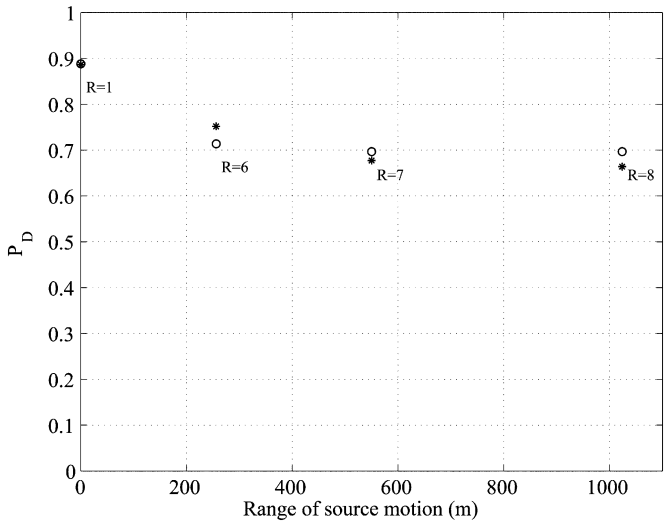

Fig. 4. Illustration of the effect of source position uncertainty on detection performance with simulated data, by plotting P_D as a function of increasing uncertainty in source range, for $P_F = 0.1$ and for about 10-dB SNR at the receivers. The ranges of source position uncertainty are defined in Table I. Solid: analytical approach. Star: Monte Carlo approach.

approach, 5000 data samples were generated for each hypothesis to produce the samples of the likelihood ratio λ using (11) and to compute P_F and P_D using (28)

$$P_F(\beta) = \int_\beta^\infty d\lambda p(\lambda \mid H_0)$$
$$P_D(\beta) = \int_\beta^\infty d\lambda p(\lambda \mid H_1). \quad (28)$$

For the analytical approach as in (22), the SNR was computed using (9) and (23). The rank R was estimated from the signal matrix using a threshold of 5% of the maximum eigenvalue.

Fig. 2 illustrates P_D as a function of SNR for Scenarios A and C. The solid curves are the analytical ROCs and the stars are the ROCs obtained using the Monte Carlo approach [5] for the Bayesian detector shown in (11). Fig. 2 shows that the analytical ROC predictions agree with the Monte Carlo predictions for both the known source range scenario A and the uncertain source range scenario C. The difference between the curves for Scenarios A and C reflects the performance degradation due to source range uncertainty. Fig. 3 compares the analytical and Monte Carlo approaches by plotting P_D as a function of P_F using normal–normal coordinates, for about 10-dB SNR at the receivers for Scenarios A and C. The normal–normal coordinates produce a linear function when the underlying distributions of the test statistic are normal. Again, the analytical and the Monte Carlo approaches agree well for both scenarios. The results demonstrate that rapid Bayesian detection performance prediction can be achieved by capturing two fundamental parameters in the proposed analytical ROC expression: The rank of the signal matrix that represents the level of source position uncertainty, and the SNR at the receivers that represents the combined effect of source level, noise level, and propagation loss.

Fig. 4 illustrates the effect of uncertain source position parameters by plotting P_D as a function of increasing source position uncertainty (Scenarios A–D) for $P_F = 0.1$ and for about 10-dB SNR at the receivers. The circles denote the analytical results. The estimated rank of the signal matrix is illustrated in the plot. The stars denote Monte Carlo computations. It shows that the performance of the Bayesian detector gradually degrades with increasing source position uncertainty. From Scenario C to D, where the uncertain ranges of source range are 550 m and 1034 m, respectively, the performance degradation of the Bayesian detector is hardly noticeable. Fig. 4 further illustrates that the effect of source position uncertainty is well-predicted by the analytical ROC expression, which can be computed much faster than using the Monte Carlo approach.

B. Experimental Results

The analytical ROC expression is further verified using the real SWellEx-96 event S5 data, by comparing the analytical predictions with the ROCs computed using the distributions of the samples of the test statistic. The latter approach is referred to as the experimental approach. It is similar to a Monte Carlo performance evaluation approach except that the test statistic samples are calculated with the experimental data not simulated data.

In the 75 min data of event S5, a total of 13 500 time-domain snapshots were generated for each of 21 array elements. Each time-domain snapshot has 1000 points, occupying 2/3 s, with 50% overlap between successive snapshots. An 8192 length fast Fourier transform (FFT) is performed on each snapshot to generate 13 500 frequency-domain spatial data vectors for each frequency bin under consideration. A data frame consists of 900 successive spatial vectors, occupying 5 min, over which the source progresses about 750 m at 2.5 m/s speed. A single ROC result is computed using a frame of the H_1 data and a frame of the corresponding H_0 data. With a series of data frames, more ROC results can be obtained.

The 109-Hz frequency data is selected as the signal data because of its high SNR. One important characteristic of the 109-Hz data is the match between the data and the wavefronts predicted using the acoustic transfer function as in (2) and the *a priori* shallow-water environmental parameters (Fig. 1). Fig. 6 plots the time-evolving source trajectory in range and depth (dashed curve), which was estimated using a conventional Bartlett processor with the 109-Hz data. Details of the source

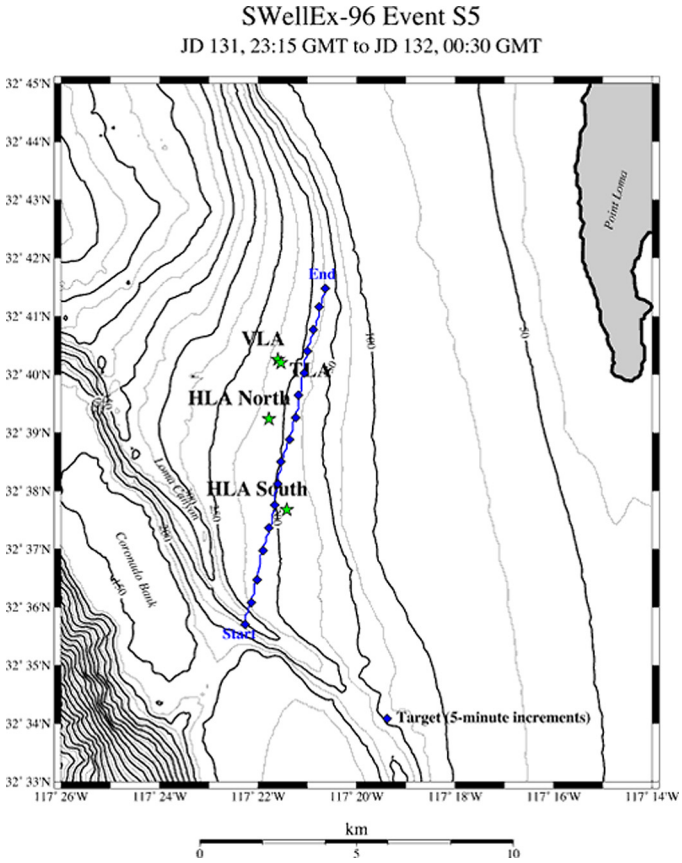

Fig. 5. Map of the source trajectory. (Color version available online at http://ieeexplore.ieee.org.)

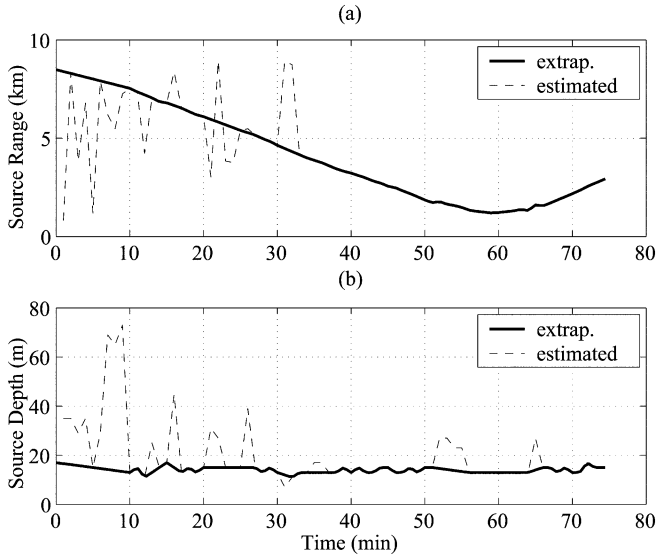

Fig. 6. Estimated and extrapolated source trajectories in range and depth for event S5 during the SWellEx-96 experiment. The estimated trajectory is obtained using a conventional Bartlett processor with SWellEx-96 environmental parameters shown in Fig. 1. Dashed: estimated. Solid: extrapolated.

trajectory estimation can be found in [20]. The estimated source trajectory between 35–75 min agrees with that computed from the GPS data, indicating that the wavefront prediction and the *a priori* environmental model is reliable. The estimated source trajectory is inaccurate between 0–35 min, mainly due to large propagation loss. To get an accurate source trajectory from the estimated trajectory, the estimated points with large deviations are manually removed. An extrapolated trajectory is obtained by filling in the missing points using linear extrapolation. The extrapolated trajectory, denoted by solid curves in Fig. 6, is used next as the *a priori* source positions. Another important characteristic of the 109-Hz data is that the source level is fixed. In this case, assuming an uncertain source amplitude with Rayleigh distribution [8] can cause performance prediction error. Here we assumed fixed source amplitude in the detection model.

Since the 109 Hz acoustic source was always on during event S5, we do not have the 109-Hz noise-only data. In addition, a second source was towed at a depth of about 54 m during event S5, transmitting numerous tonals that span the frequencies between 49–400 Hz. To avoid the interference from the second source, the 99-Hz frequency data is selected to represent the diffuse noise field. It does not overlap with any source frequency and it is close to 109 Hz.

A weighted sum of the 109-Hz and 99-Hz data is used as the signal-plus-noise data for the H_1 hypothesis

$$\begin{aligned} H_1 &: \mathbf{r}_1 = \mathbf{r}_{109} + a_i \mathbf{r}_{99} \\ H_0 &: \mathbf{r}_0 = b_i \mathbf{r}_{99} \end{aligned} \tag{29}$$

where $\mathbf{r}_{109}$ and $\mathbf{r}_{99}$ means 109-Hz and 99-Hz spatial data vectors. The coefficient a_i is assigned to adjust the noise level of the ith data frame so that the detection performance can be evaluated at a wide range of SNRs. The coefficient b_i is used to prevent the effect of noise level mismatch. It is calculated by equalizing the total noise energy in a frame of $\mathbf{r}_1$ and the total noise energy in the corresponding frame of $\mathbf{r}_0$

$$\begin{aligned} b_i &= \frac{\sum_{j=1}^{900} \|\mathbf{r}_{1\perp_{ij}}\|^2}{\sum_{j=1}^{900} \|\mathbf{r}_{99\perp_{ij}}\|^2} \\ \mathbf{r}_{\perp_{ij}} &= \mathbf{r} - \mathbf{s}(\mathbf{\Psi}, \mathbf{S}_{ij})^{\dagger} \mathbf{r} \mathbf{s}(\mathbf{\Psi}, \mathbf{S}_{ij}) \end{aligned} \tag{30}$$

where $\mathbf{r}_{\perp_{ij}}$ denotes the portion of the jth spatial vector in the ith data frame (either $\mathbf{r}_1$ or $\mathbf{r}_{99}$) that is orthogonal to the predicted signal wavefront $\mathbf{s}(\mathbf{\Psi}, \mathbf{S}_{ij})$. The source position $\mathbf{S}_{ij}$ corresponds to the jth spatial vector in the ith data frame.

Although this is a synthetic way of obtaining the H_1 and H_0 data, it preserves the wavefront uncertainty in the data and preserves source motion as the primary cause of wavefront uncertainty, which is the focus of this paper. The analytical performance prediction approach is verified by comparing the analytical prediction result with experimental prediction result, by comparing the results across various data frames, and by comparing the performance prediction for the Bayesian detector with that for the energy detector and the mean-ocean detector. A series of $\mathbf{r}_1$ and $\mathbf{r}_0$ data frames along the entire event S5 trajectory are used. In constructing the synthetic data, a_i is first assigned to be 1.6 for all data frames and b_i is calculated for each data frame using (30). Other a_i values can also be used to construct the data, which is discussed below.

Two scenarios are considered. In Scenario I, accurate source position for each snapshot is assumed known *a priori*, which is obtained from the extrapolated source trajectory (Fig. 6). The

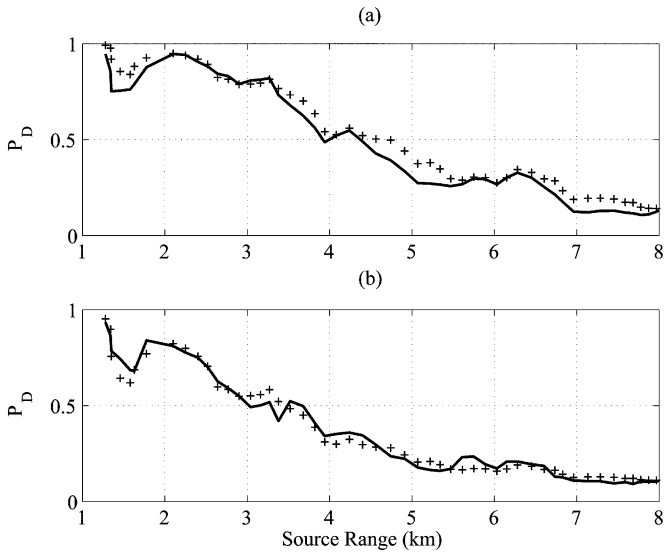

Fig. 7. Illustration of the analytical performance prediction and experimental performance prediction for the Bayesian detector with the data collected during event S5 in the SWellEx-96 experiment. The P_D result is plotted as a function of the center of the source range across data frames, given $P_F = 0.1$. Solid: experimental approach. Plus: analytical prediction approach. (a) Scenario I. (b) Scenario II.

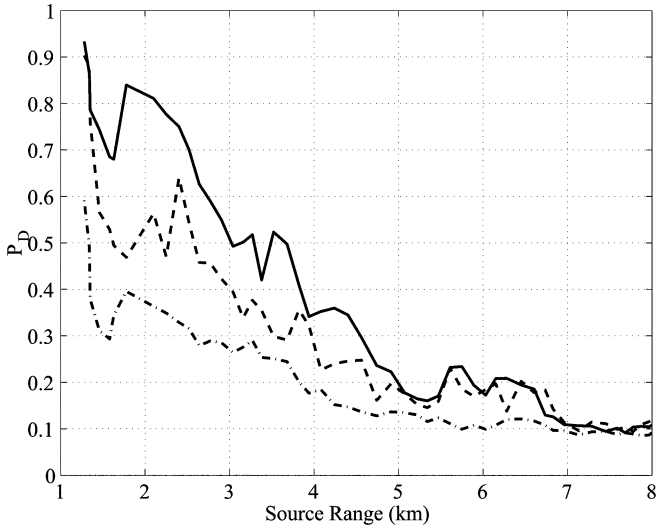

Fig. 8. Illustration of experimental performance prediction for various detectors with the data collected during event S5 in the SWellEx-96 experiment. The P_D result is plotted as a function of the center of the source range across data frames, given $P_F = 0.1$. Solid, dashed, and dash-dotted curves denote the P_D results for the Bayesian detector, the mean-ocean detector, and the energy detector for Scenario II, respectively.

performance prediction for the Bayesian detector for this scenario provides a performance upper bound. In Scenario II, the region of uncertain source position for each H_1 data frame is assumed known *a priori*, which is an area of 750 $\times$ 4 m. The analytical performance prediction approach captures the performance degradation caused by the limited *a priori* knowledge about source position, and provides a rapid and realistic P_D prediction.

Fig. 7 plots the P_D prediction results for the Bayesian detectors as a function of the center of the source range of the data frames, given $P_F = 0.1$. In Fig. 7(a), Scenario I is considered. The solid curve denotes experimental evaluation results for the matched-ocean detector, obtained using (24) to generate the distribution of the likelihood ratio for each data frame. The signal wavefront is predicted using (2) and the known source position and ocean parameters. The plus denotes the analytical P_D results computed using (25) with parameter SNR_i estimated from the ith data frame using the following empirical formula

$$\begin{aligned} \mathrm{SNR}_i &= N\frac{E_{1i} - E_{0i}}{E_{0i}} \\ E_{1i} &= \sum_{j=1}^{900} \|\mathbf{r}_{1ij}\|^2 \\ E_{0i} &= \sum_{j=1}^{900} \|\mathbf{r}_{0ij}\|^2 \end{aligned} \tag{31}$$

where $\mathbf{r}_{1ij}$ and $\mathbf{r}_{0ij}$ are the jth spatial vector in the ith data frame of $\mathbf{r}_1$ and $\mathbf{r}_0$, respectively. In Fig. 7(b), Scenario II is used. The solid curve represents experimental P_D result for the Bayesian detector, obtained using (11). The signal matrix used in (11) consists of 120 realizations of the signal wavefront due to 120 source positions uniformly spaced in the *a priori* region (750 m $\times$ 4 m) for 40 range increments and 3 depth increments.

The SNR parameter is the same as that used for the matched-ocean detector for Scenario I. The pluses denote analytical P_D results computed using (22), given $P_F = 0.1$. The analytical approach uses the same SNR parameters and signal matrix that are used in the experimental method. The parameter R is estimated from the signal matrix using a threshold that equals 5% of the maximum eigenvalue. As shown in Fig. 4, R increases gradually from 7 to 8 when the range of source range uncertainty increases from 550 to 1000 m. Since the variation of R across data frames is small, an averaged $R = 7$ is used for all data frames. This R value is associated with source range uncertainty of 750 m due to source motion in 5 min at 2.5 m/s. Note that the R also depends on uncertainty in ocean environmental parameters. Here the ocean parameters are known accurately, so the R reflects source range uncertainty only.

Fig. 7 shows that the analytical prediction P_D results agree with the experimental evaluation results over most of the event S5 track, for both scenarios. The consistency of the results is a good demonstration of the analytical prediction approach. Some minor disagreements may be due to inaccurate shallow-water environment parameters assumed for the detector. The degradation of the detection performance for Scenario I to that for Scenario II is caused by the limited amount of information about the source position, which is correctly captured by the rank parameter in the analytical ROC expression.

The P_D performance of the Bayesian detector is compared with that of the mean-ocean detector and the energy detector for $P_F = 0.1$ in Fig. 8, denoted by the solid curve, the dashed curve, and the dash-dotted curve, respectively. The results for the Bayesian detector are the same as those illustrated in Fig. 7(b). The results for the mean-ocean detector and the energy detector are computed using (26) and (27) for Scenario II. The mean-ocean signal wavefront used by the mean-ocean detector is predicted using the center source position for each data frame and the known ocean parameters. The results presented in Fig. 8 show that the performance of the Bayesian

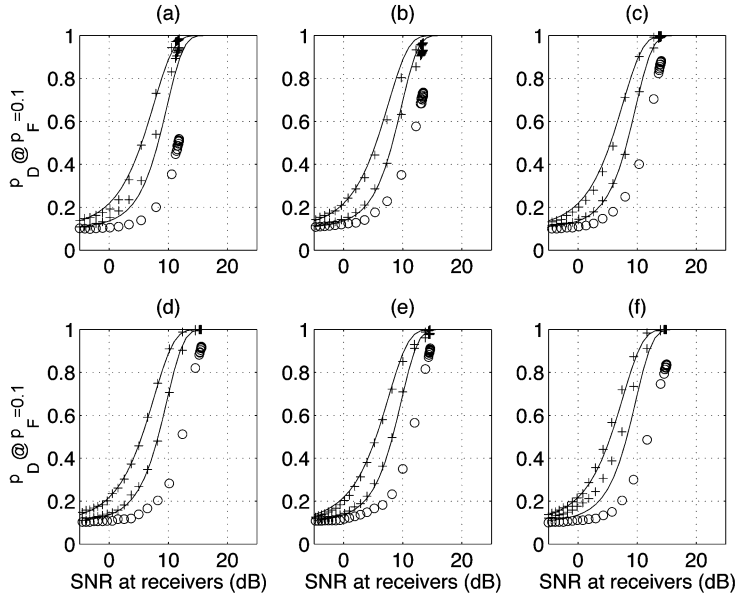

Fig. 9. Illustration of the analytical performance prediction and experimental performance prediction for the Bayesian detector with SWellEx-96, event S5 data. The P_D result is plotted as a function of SNR for $P_F = 0.1$. Solid: analytical results, plus: experimental results. Left: Scenario I, known signal wavefronts. Right: Scenario II, uncertain signal wavefronts. Circle: experimental performance results for the energy detector. Data frames are associated with the source trajectory start at (a) 30 min ($\mathrm{SR} = 4641\,\mathrm{m}$), (b) 35 min ($\mathrm{SR} = 3881\,\mathrm{m}$), (c) 40 min ($\mathrm{SR} = 3221\,\mathrm{m}$), (d) 45 min ($\mathrm{SR} = 2561\,\mathrm{m}$), (e) 65 min ($\mathrm{SR} = 1598\,\mathrm{m}$), and (f) 70 min ($\mathrm{SR} = 2179\,\mathrm{m}$). SR means the source range.

detector is better than those of the mean-ocean detector and the energy detector, because the Bayesian detector incorporates the *a priori* source position information in an optimal way.

The results shown in Figs. 7 and 8 are associated with the data frames synthesized using a fixed coefficient $a_i = 1.6$. It is important to verify the analytical prediction approach against different values of the coefficient a_i. By varying a_i from 0.4 to 16, and changing b_i accordingly using (30), additional data frames were synthesized as in (29), and were used to check the analytical prediction approach. The SNRs were estimated from the data frames using (31). Since the SNR of the data frame depends on the coefficient a_i and is physically meaningful, the results are illustrated in Fig. 9 by plotting the predicted P_D as a function of the SNR. In Figs. 9(a)–(f), the data frames are corresponding to pieces of the source trajectory starting at 30, 35, 40, 45, 65, and 70 min, with corresponding source ranges at 4641, 3881, 3221, 2561, 1598, and 2179 m, respectively, given $P_F = 0.1$. The solid curves are the analytical prediction P_D results obtained using (22) for Scenario I and (25) for Scenario II. The pluses are experimental evaluation P_D results, computed using (24) and (11) for Scenarios I and II, respectively. The circles denote experimental evaluation results for the energy detector for Scenario II. Fig. 9 shows that the analytical and experimental P_D versus SNR curves agree with each other. The agreement is consistent across various data frames. It indicates that the detection model is feasible in characterizing the data in a real circumstance. It further indicates that the performance of the Bayesian detector in the presence of source position uncertainty can be rapidly predicted by the proposed analytical ROC expression. The difference between analytical and experimental results might be due to model parameter mismatch, SNR estimation error, and a limited number of trials for experimental evaluation.

VII. Discussion and Summary

If the environmental parameters are precisely measured and the acoustic signal wavefront is accurately modeled and predicted, environmental uncertainty can be avoided. However, it is usually difficult to get an accurate description of the target position and the ocean parameters. What can often be obtained are the ranges of possible values of uncertain environmental parameters, such as "water depth is 100 ± 5 m." Our approach translates the *a priori* ranges of uncertain environmental parameters to uncertainty in the signal wavefront, and then develops the ROC expressions for predicting the Bayesian detection performance.

The analytical Bayesian ROC expression presented in this paper predicts the detection performance degradation caused by environmental source position uncertainty. Although the simulation and experimental verifications in this paper focus only on source position uncertainty caused by source motion, the application of the analytical ROC expression is not limited to these cases. It can be extended to various other environmental uncertainty scenarios [8]. In summary, we have developed an approach for translating environmental uncertainty into detection performance prediction. In particular, the detection model and the ROC expressions are verified for both simulated data and real experimental data in which there is signal wavefront uncertainty caused by source position uncertainty. The simulation results demonstrate that the analytical ROC expression yields accurate and faster performance prediction as compared to conventional experimental performance evaluation approach, as least for the test cases. The analytical prediction results obtained using the SWellEx96 experimental data show that the signal source model and the acoustic propagation

model are practical. The analytical ROC expression for the Bayesian detector can be applied in a realistic circumstance to provide fast detection performance prediction in which there is environmental uncertainty.

ACKNOWLEDGMENT

The authors would like to thank Dr. J. L. Krolik and Dr. Yifang Xu for helpful discussions on the detection model, and Dr. W. S. Hodgkiss of the Marine Physics Laboratory, Scripps Institution of Oceanography, for providing the SWellEx-96 data.

REFERENCES

[1] E. C. Shang, "Environmental mismatching effects on source localization processing in mode space," *J. Acoust. Soc. Amer.*, vol. 89, no. 5, pp. 2285–2290, Nov. 1991.

[2] A. Tolstoy, "Sensitivity of matched-field processing to sound-speed profile mismatch for vertical arrays in a deep-water pacific environment," *J. Acoust. Soc. Amer.*, vol. 85, no. 6, pp. 2394–2404, Jun. 1989.

[3] G. B. Smith, H. A. Chandler, and C. Feuillade, "Performance stability of high-resolution matched-field processors to sound-speed mismatch in a shallow-water environment," *J. Acoust. Soc. Amer.*, vol. 93, no. 5, pp. 2617–2626, Mar. 1993.

[4] A. M. Richardson and L. W. Nolte, "A posteriori probability source localization in an uncertain sound speed, deep ocean environment," *J. Acoust. Soc. Amer.*, vol. 89, no. 5, pp. 2280–2284, May 1991.

[5] J. A. Shorey, L. W. Nolte, and J. L. Krolik, "Computationally efficient Monte Carlo estimation algorithm for matched field processing in uncertain ocean environments," *J. Comput. Acoust.*, vol. 2, no. 3, pp. 285–314, Sep. 1994.

[6] V. Premus, D. Alexandrou, and L. W. Nolte, "Full-field optimum detection in an uncertain, anisotropic random wave scattering environment," *J. Acoust. Soc. Amer.*, vol. 98, no. 2, pp. 1097–1110, Aug. 1995.

[7] M. Wazenski and D. Alexandrou, "Active, wideband detection and localization in an uncertain multipath environment," *J. Acoust. Soc. Amer.*, vol. 101, no. 4, pp. 1961–1970, Oct. 1997.

[8] L. Sha and L. W. Nolte, "Effects of environmental uncertainties on sonar detection performance prediction," *J. Acoust. Soc. Amer.*, vol. 117, no. 4, pp. 1942–1953, Apr. 2005.

[9] ——, "Bayesian sonar detection performance prediction in the presence of interferences in uncertain environments," *J. Acoust. Soc. Amer.*, vol. 117, no. 4, pp. 1954–1964, Apr. 2005.

[10] F. B. Jensen, W. A. Kuperman, M. B. Porter, and H. Schmidt, *Computational Ocean Acoustics, AIP Series in Modern Acoustics and Signal Processing*. New York: AIP Press, 1994.

[11] M. B. Porter, *The KRAKEN Normal Mode Program*. La Spezia, Italy: SACLANT Undersea Research Centre, 1991.

[12] L. A. Wainstein and V. D. Zubakov, *Extraction of Signals From Noise*. Englewood Cliffs, NJ, USA: Prentice-Hall, 1962, pp. 296–299.

[13] L. E. Brennan and I. S. Reed, *Theor. Adaptive Radar*, vol. AES-9, no. 2, pp. 237–252, Mar. 1973.

[14] S. M. Kay, *Fundamentals of Statistical Signal Processing: Detection Theory*, ser. Prentice Hall Signal Processing. Englewood Cliffs, NJ: Prentice Hall, 1998, pp. 71–72.

[15] J. I. Marcum and P. Swerling, "Studies of target detection by pulsed radar," *IRE Trans. Inf. Theory*, vol. IT-6, Apr. 1960.

[16] Z. Bai, J. Demmel, J. Dongarra, A. Ruhe, and H. van der Vorst, and eds., *Templates for the Solution of Algebraic Eigenvalue Problems: A Practical Guide*. Philadelphia, PA: SIAM, 2000.

[17] T. H. Cormen, C. E. Leiserson, and R. L. Rivest, *Introduction to Algorithms*. New York: McGraw-Hill and the MIT Press, 1998.

[18] W. S. Burdic, *Underwater Acoustic System Analysis*, ser. Signal processing. Englewood Cliffs, NJ: Prentice-Hall, 1984.

[19] N. O. Booth, A. T. Abawi, P. W. Schey, and W. S. Hodgkiss, "Detectability of low-level broad-band signals using adaptive matched-field processing with vertical aperture arrays," *IEEE J. Ocean. Eng.*, vol. 25, no. 3, pp. 296–313, Jul. 2000.

[20] H. C. Song, J. De Rosny, and W. A. Kuperman, "Improvement in matched field processing using the clean algorithm," *J. Acoust. Soc. Amer.*, vol. 113, no. 3, pp. 1379–1386, Mar. 2003.

Liewei Sha received the B.S. degree in electronic engineering from Tsinghua University, Beijing, China, in 1995, the M.S. degree in signal processing from Institute of Acoustics, the Chinese Academy of Sciences, Beijing China, in 1998, and the Ph.D. degree in electrical and computer engineering from Duke University, Durham, NC, in 2004.

Since 2003, she has been an Engineer with Magnetic Resonance Imaging, GE Healthcare Technology, Waukesha, WI. Her research interests are in the area of digital signal processing and statistical signal processing with applications to diagnostic imaging and underwater acoustics.

Dr. Sha is a Member of the International Society for Magnetic Resonance in Medicine.

Loren W. Nolte (S'56–M'57–LM'99–LS'01) was born in Napoleon, OH. He received the B.S.E.E. degree from Northwestern University, Evanston, IL, and the M.S.E. degree and Ph.D. degree, in 1965, from The University of Michigan, Ann Arbor, all in electrical engineering.

Following a year of postdoctoral research in signal detection theory at The University of Michigan, he joined the faculty at Duke University, Durham, NC, as an Assistant Professor of Electrical Engineering and became a Professor of Electrical and Biomedical Engineering in 1972. He has held Visiting Professorships at the University of Colorado, Boulder, Colorado State University, Fort Collins, the University of Washington, Seattle, and the Scripps Institution of Oceanography, La Jolla, CA. He was chairman of the Department of Electrical and Computer Engineering at Duke from 1998 to 2001. His research interests have included optimal Bayesian approaches to adaptive detection, classification, tracking, and localization of ocean acoustics signals, including recurrent transients. His recent contributions include the development of optimal physics-based array signal processing algorithms, which incorporate the physics, as well as the uncertainty of ocean acoustic environmental parameters. He was also an early contributor to optimal (likelihood-ratio-based) decision fusion. His current research interests are in signal detection and estimation theory with applications to ocean acoustics, biomedical statistical image processing in cancer research in collaboration with the Duke University Medical Center, and optimal decision fusion.

Dr. Nolte has served as an Associate Editor of underwater acoustics for the IEEE TRANSACTIONS ON ACOUSTICS, SPEECH, AND SIGNAL PROCESSING, and he also served on its Technical Committee on Underwater Acoustics.